ACS APPLIED MATERIALS & INTERFACES

www.acsami.org

Research Article

PEG@ZIF-8/PVDF Nanocomposite Membrane for Efficient Pervaporation Desulfurization via a Layer-by-Layer Technology

Hexiang Sun, Zachary Magnuson, Wenwen He, Weijie Zhang, Harsh Vardhan, Xiaolong Han,* Gaohong He,* and Shengqian Ma*

Cite This: *ACS Appl. Mater. Interfaces* 2020, 12, 20664−20671

Read Online

ACCESS | Metrics & More | Article Recommendations | Supporting Information

ABSTRACT: The desulfurization property of conventional mixed matrix membranes (MMMs) cannot meet the necessary demand due to particles aggregation and interface defects. Here, we put forward a layer-by-layer (LBL) approach to make a novel PEG@ZIF-8/poly(vinylidene difluoride)-(PVDF) composite membrane for pervaporation desulfurization. In this way, a ZIF-8 layer is covered on the surface of the PVDF porous membrane via an in situ growth method. Then, a PEG layer is covered on the ZIF-8 layer by a casting method. Compared with pristine PEG membranes, the separation performance of the ZIF-8@PEG/PVDF nanocomposite membrane increased significantly. This can be attributed to the homogeneous ZIF-8 particle layer and better compatibility between the poly(ethylene glycol) (PEG) matrix and ZIF-8 particles. The membrane achieves a maximum total flux of 3.08 kg·m^{-2}·h^{-1} at the third in situ growth cycles of ZIF-8 particles and a maximum sulfur enrichment factor of 7.6 at the sixth in situ growth cycles of ZIF-8 particles.

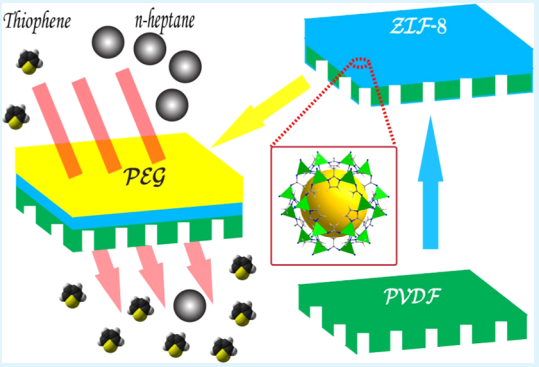

KEYWORDS: *metal−organic framework, ZIF-8 nanoparticles, layer-by-layer, nanocomposite membrane, pervaporation desulfurization, separation*

1. INTRODUCTION

Recently, the combustion of sulfur-containing gasoline has become a cause of severe smog, which is harmful to human health, leading to increasingly more stringent automotive fuel standards.[1] In Europe, the United States, and China, the sulfur content of gasoline for motor vehicles has been constrained to 10 ppm. Several desulfurization technologies[2−6] have been employed, but these high-energy consumption methods cannot fully meet the industrial demand of desulfurization. It appears important to address the problem at its source to formulate the most effective solutions.

Pervaporation, as a low-energy consumption separation technology, has become an attractive desulfurization method by virtue of easy coupling with other operating processes and its negligible effect on fuel octane rating.[7,8] The key to pervaporation desulfurization is to research robust membranes. Using the solubility parameter theory, Lin et al. selected poly(ethylene glycol) (PEG) as the membrane material and prepared a cross-linked PEG membrane, showing that the PEG membrane had excellent desulfurization property.[9] Poly-(dimethylsiloxane) (PDMS) is another widely known desulfurization membrane, and myriad inorganic particles have been employed as fillers to enhance the property of PDMS membrane. For instance, Li et al.[10] prepared PDMS-AgY molecular sieves mixed matrix membranes (MMMs), and Jiang et al.[11] prepared Ni^{2+}Y zeolite molecular sieves MMMs. Other desulfurization polymer membranes like polyimides (PI),[12] poly(ether-*block*-amide) (PEBAX),[13] and polyphosphazene (POP)[14] have also been reported.

Metal−organic frameworks (MOFs), a kind of coordination polymers, are self-assembled from organic ligands and metal ions via self-assembly, having a periodic network structure, permanent porosity, large specific surface area, and adjustable pore structure. By virtue of these characteristics, MOFs have been well applied in pervaporation, gas storage, separation,[15−17] etc. Jiang et al. prepared MMMs with PDMS polymer matrix and two MOFs as fillers (MIL-101 and CuBTC) and applied them to model gasoline desulfurization.[18,19] The results showed that the MOF particles-filled PDMS membrane showed better desulfurization than the pristine PDMS membrane, owing to the high thiophene-adsorption selectivity induced by the MOF. However, the aggregation of MOF particles and interface defects limited the performance of MMMs at high-loading fillers. Several methods have been proposed to overcome this: an amine-functionalized

Received: February 9, 2020
Accepted: March 31, 2020
Published: March 31, 2020

https://dx.doi.org/10.1021/acsami.0c02513
ACS Appl. Mater. Interfaces 2020, 12, 20664−20671

MOF, NH_2-MIL-125 (Ti), was employed to fabricate MMMs, the MOF accounting for up to 30 wt %, and the MMMs effectively increased the permeability of CO_2 and CH_4.[20] In addition, a new preparation process was employed to minimize the adverse effect. For example, the research results of Deng et al.[21] and our group[22] showed that this was a very efficient method due to the use of the same solvent as that used in the MOF synthesis and solution of the polymer membrane materials. Besides, Wang et al. fabricated a polyamide/ZIF-8 composite membrane by layer-by-layer (LBL) method followed by nanofiltration, showing that the PA/ZIF-8 membrane showed excellent performance for dye removal.[23]

Herein, we provide a method of fabrication for the PEG@ZIF-8/poly(vinylidene difluoride)(PVDF) LBL membrane used in pervaporation desulfurization. First, ZIF-8 nanoparticles were fabricated by a water-based process and uniformly dispersed in water. From this, PVDF substrate was introduced, and ZIF-8 nanoparticles grew at the surface forming a dense ZIF-8 layer. Then, the PEG solution was cast on the ZIF-8 layer to form a dense PEG layer. The schematic of the preparation is shown in Figure 1. The desulfurization

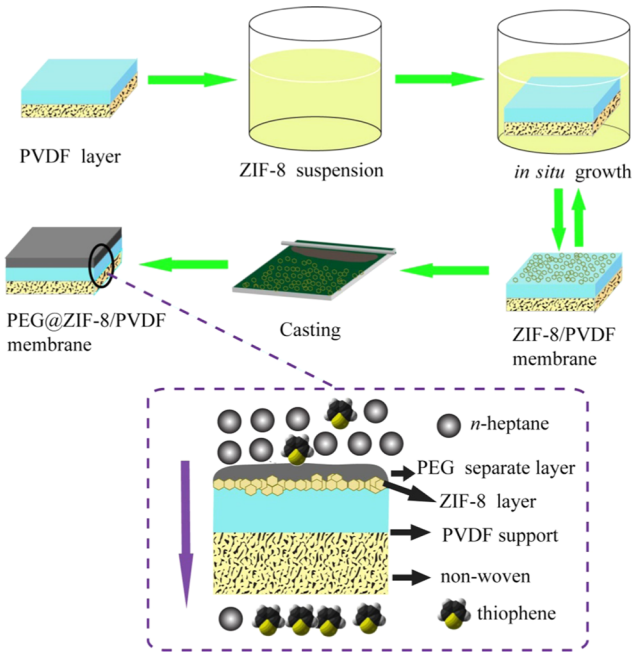

Figure 1. Schematic of fabrication of the PEG@ZIF-8/PVDF nanocomposite membrane.

property of the prepared membrane was estimated by separating simulated gasoline consisting of thiophene and *n*-heptane. The effects of the cycles of ZIF-8 particles on in situ growth, feed temperature, and feed thiophene content were investigated in detail.

2. EXPERIMENTAL SECTION

2.1. Materials. Poly(ethylene glycol) (PEG, MW = 100 000) was supplied by Sigma-Aldrich, and *n*-heptane and thiophene were purchased from Aladdin Industrial Corporation. Trimethylamine solution (30 wt %) was supplied by Adamas Reagent Co. Ltd. Zinc nitrate hexahydrate and 2-methylimidazole were obtained from Fuchen Chemical (Tianjin, China) and Adamas Reagent Co. Ltd., respectively.

2.2. Preparation of Membrane. *2.2.1. Preparation of ZIF-8 Suspension.* For the preparation of ZIF-8 particles and ZIF-8 suspension, refer to our previous work.[22]

2.2.2. Fabrication of PEG@ZIF-8/PVDF Nanocomposite Membranes. The assembled membrane was synthesized by an in situ growth method. For a typical procedure, ZIF-8 suspension was transferred to a polymethyl methacrylate (PMMA) plate container, then the PVDF support membrane was completely immersed in the ZIF-8 suspension for 12 h forming a ZIF-8 layer, which was washed thoroughly with deionized water and then dried at 50 °C for 1.5 h. The prepared membrane was marked as ZIF-8/PVDF#1. The above steps of ZIF-8 layer formation were repeated one−five times to obtain ZIF-8/PVDF(#2−6), respectively.

The PEG layer was prepared as follows: First, 1.5 g of PEG powder was dissolved in a 9 g aqueous solution of ethanol (50 wt %). Then, 0.24 g of maleic anhydride and 0.045 g of trimethylamine were added while stirring. The mixed liquor was cast on the prepared ZIF-8/PVDF(#1−6) support membranes to obtain a nanocomposite-assembled membrane PEG@ZIF-8/PVDF(#1−6). Finally, these PEG@ZIF-8/PVDF(#1−6) membranes were dried at room temperature for 1 day to ensure the solvent was completely removed and then cross-linked in an oven at 80 °C for 5 h.

2.3. Characterization of Membrane. Fourier transform infrared (FT-IR) spectroscopy was carried out using a FT-IR spectrometer (Bruker, Germany). The morphology of ZIF-8 particles and membranes was determined by scanning electron microscopy (SEM; ZEISS, Germany). The surface chemical composition of ZIF-8 nanocomposite membranes was analyzed by X-ray photoelectron spectroscopy (XPS; Kα, UK). The crystal structures of the ZIF-8 particles and ZIF-8 nanocomposite membranes were characterized by X-ray diffraction (XRD) (D8; Bruker, Germany).

2.4. Pervaporation Experiments. The pervaporation performance was evaluated using our self-made device shown in Figure S1. The feed liquid was simulated gasoline consisting of thiophene and *n*-heptane. The feed liquid was passed through the membrane to the permeate side under the differential pressure maintained around 300 Pa via a vacuum pump. The pervaporation performance was evaluated using permeate flux and sulfur enrichment factor; for the calculation formula, refer to our previous work.[22]

3. RESULTS AND DISCUSSION

3.1. Characterization of ZIF-8 Particles and Membranes. *3.1.1. Characterization of ZIF-8 Particles.* Figure 2a shows that the characteristic diffraction peaks at 7.3, 10.3, 12.7,

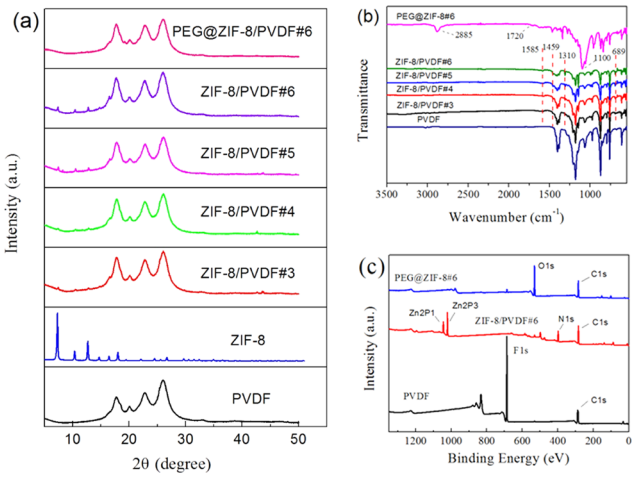

Figure 2. (a) XRD of PVDF, ZIF-8, ZIF-8/PVDF(#3−6), and PEG@ZIF-8/PVDF#6 membranes. (b) FT-IR of PVDF, ZIF-8/PVDF(#3−6), and PEG@ZIF-8/PVDF#6 membranes. (c) XPS of PVDF, ZIF-8/PVDF#6, and PEG@ZIF-8/PVDF#6 membranes.

https://dx.doi.org/10.1021/acsami.0c02513
ACS Appl. Mater. Interfaces 2020, 12, 20664−20671

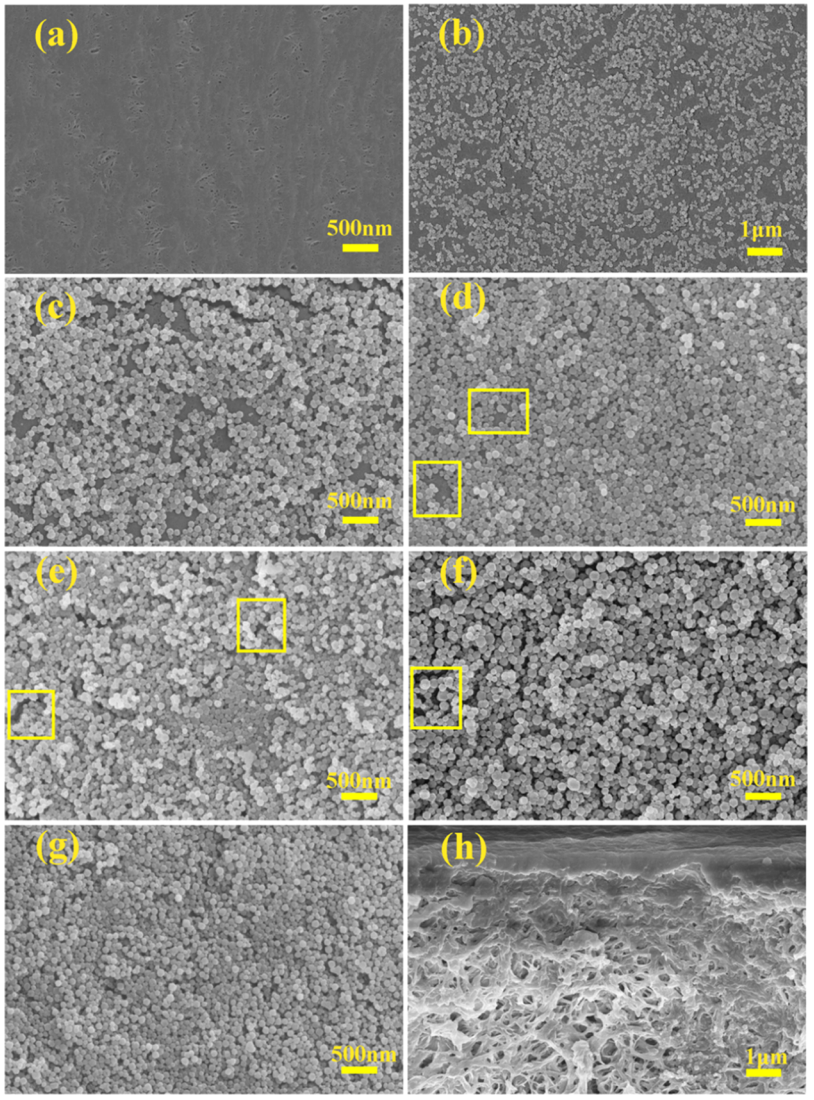

Figure 3. Surface SEM images of the PVDF membrane (a) and the ZIF-8/PVDF membranes (b−g, #1−6) and the cross-sectional SEM image of ZIF-8/PVDF#6 membrane (h).

14.6, 16.4, and 18.1° correspond to ZIF-8 peaks in the JPCDS card numbers 011, 002, 112, 022, 013 and 222 demonstrating that the prepared nanoparticles are ZIF-8 crystals.[24−26] The N_2 adsorption−desorption isotherms and pore size distribution are shown in Figures S2 and S3, respectively. The Brunauer−Emmett−Teller (BET) surface area of the prepared ZIF-8 particles is 1472 m^2 g^{-1}. Figure S4 indicates that the ZIF-8 particles as synthesized exhibit a regular dodecahedron structure with a size of 30−100 nm, which is very important for the preparation of uniformly dispersed ZIF-8 layer. Transmission electron microscopy (TEM) was also used to characterize the morphology of ZIF-8 particles. Figure S5 shows that ZIF-8 nanocrystals have good pore structures and their average particle size distribution is about 50 nm.

3.1.2. ZIF-8 Nanocomposite Membranes Characterization. The XRD spectra of PVDF, ZIF-8/PVDF(#3−6), and PEG@ZIF-8/PVDF#6 membranes are illustrated in Figure 2a. The peaks at 18.4 and 26.7° are assigned to the α phase of PVDF.[27] The peak at 20.6° is assigned to the β phase of PVDF.[28] Compared to the pristine PVDF membrane, three new characteristic peaks at 7.3, 10.4, and 12.7° appeared after in situ growth of ZIF-8 particles. Besides, the intensity of these characteristic peaks increases with the number of in situ growth cycles. These characteristic peaks of ZIF-8 disappear after casting PEG solution, indicating that a uniform and compact PEG layer covers the ZIF-8 layer. The dense, uniform, and defect-free PEG layer is very important to the pervaporation desulfurization.

The FT-IR spectroscopy results are shown in Figure 2b. The peaks at 1310, 1585, and 1459 cm^{-1} correspond to N−H bending vibration, C═N stretching vibration, and C−N stretching vibration of ZIF-8.[29,30] The characteristic peaks of ZIF-8 appear on both ZIF-8/PVDF membranes, and the intensity of peaks increases with an increase in the number of in situ growth cycles. The ZIF-8 characteristic peak at 1310 cm^{-1} disappears on the spectra of the PEG@ZIF-8/PVDF#6 membrane, and new characteristic peaks at 2885, 1100, and 1720 cm^{-1} corresponding to axial deformations of C−H, C−O, and C═O of PEG appear,[31] further showing that the ZIF-8 layer is completely covered by the PEG separation layer.

To elucidate the surface composition of the membranes, XPS experiments were carried out and are shown in Figure 2c. In comparison to the pure PVDF membrane, the peak of F1s disappears and the peaks $Zn2p_{3/2}$ at 1021.1 eV and $Zn2p_{1/2}$ at

https://dx.doi.org/10.1021/acsami.0c02513
ACS Appl. Mater. Interfaces 2020, 12, 20664−20671

1044.2 eV appear,[32] showing that the ZIF-8 layer completely covers the PVDF support membrane and forms a dense ZIF-8 layer. After coating in PEG solution, the O1s peak appears and the peaks Zn2p1 and Zn2p3 disappear, demonstrating that the PEG select layer completely covers the ZIF-8 layer and forms an LBL PEG@ZIF-8/PVDF membrane.

Figure 3a presents the surface image of the PVDF support membrane; many nanopores can be seen on the PVDF membrane surface. Figure 3b shows that only parts of the PVDF membrane is overlapped by ZIF-8 particles, and they are easily separated from the surface. This is because ZIF-8 particles are difficult to grow on the smooth surface of the PVDF membrane. After the first procedure of ZIF-8 in situ growth, the surface of the membrane loses its smooth quality, so the ZIF-8 particles that adhere to the surface seed additional growth.[33] Thus, the ZIF-8 particles are easy to grow on the surface of the ZIF-8/PVDF#1 membrane. It can be seen that the ZIF-8 layer density increases with the number of in situ growth cycles (Figure 3b–g). After the sixth cycle (Figures 3g and S6a), a uniform and dense ZIF-8 layer is formed. In Figures 3h and S6b, the cross-sectional morphology of the ZIF-8/PVDF#6 membrane can be seen; there is a dense ZIF-8 layer on the surface of PVDF, and some particles infiltrate into the pores of PVDF owing to the small size of the prepared ZIF-8 particles. To study the adhesion between the ZIF-8 layer and the PVDF membrane under testing conditions, the ZIF-8/PVDF#6 membrane was immersed into *n*-heptane/thiophene mixtures for 10 days; the results are shown in Figure S7. The photos and micrographs of the ZIF-8/PVDF#6 membrane show that the ZIF-8 layer is still combined tightly after immersion in *n*-heptane/thiophene mixtures, which is very important for the stability of the membrane.

The surface and cross-sectional morphology of PEG@ZIF/PVDF(#4–6) membranes are shown in Figure S8. It can be seen that the surface of the PEG@ZIF-8/PVDF membrane becomes smoother with an increase in the number of in situ growth cycles from four to six. This is because the ZIF-8 layer becomes denser and more uniform making it easier to cast the PEG layer over the uniform supporting layer. Figure S8d–f shows that the PEG separation layers and the ZIF-8/PVDF supports are combined tightly, and a portion of PEG penetrates into the ZIF-8 layer and the PVDF support layer, helping to bind the assembled membrane.[34] The thickness of the separation layer of the ZIF-8@PEG/PVDF#6 is about 7 μm.

3.2. Pervaporation Performance of ZIF-8 Nanocomposite Membranes. *3.2.1. Effect of In Situ Growth Procedure.* To explore the effect of ZIF-8 particles' in situ growth cycles on the pervaporation desulfurization performance, the PEG@ZIF-8/PVDF nanocomposite membranes were evaluated at different stages of layer growth (1–6). As shown in Figure 4, with increasing ZIF-8 in situ growth cycles, the permeation flux first increases (1–3) and then decreases. From 1 to 3, the packing of PEG polymer chains is interrupted by the increased number of ZIF-8 particles, which create excess free-volume cavities at the interface between PEG matrix and ZIF-8 particles.[18] With additional cycles up to 3, the highest permeation flux of 3.08 kg/(m^2 h) is obtained. When the number of cycles increases from 3 to 6, the increasing number of particles gradually form a dense ZIF-8 multilayer. Figure S8 shows that there are peaks and valleys of the ZIF-8 particles layer beneath the PEG layer in the composite membrane. With the formation of the dense ZIF-8 layer, the penetration of PEG

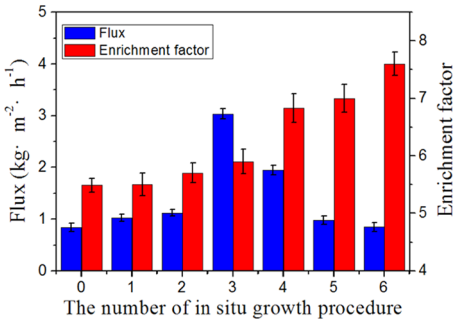

Figure 4. Effect of the number of in situ growth cycles on the desulfurization performance of membranes (the feed thiophene concentration is about 200 ppm).

is reduced, and the PEG layer is thicker than before (as observed in Figure S9). The two dense layers prevent the permeation of thiophene and *n*-heptane, lowering the permeation flux. The increased enrichment factor is determined by the combined effect of the PEG and ZIF-8 layers. With growth cycles 1–3, the permeate must pass through the PEG and ZIF-8 layers at peaks. However, the thiophene and *n*-heptane molecules only pass through the PEG layer at valleys. With growth cycles 4–6, the ZIF-8 layer becomes denser, and the thiophene and *n*-heptane molecules must pass through the PEG and ZIF-8 layers sequentially. Both PEG and ZIF-8 are shown to have high thiophene selectivity;[22,35,36] thus, the sulfur enrichment factor increases with increasing layering cycles.

3.2.2. Effect of Temperature. The influence of temperature on the desulfurization performance of the PEG@ZIF-8/PVDF#6 membrane was investigated. As shown in Figure 5a, the permeation flux appears to increase with an increase in temperature, while the enrichment factor first increases and then decreases above 75 °C. The two main reasons for the trend of permeation flux are as follows: (1) With increasing temperature, the vapor pressure and diffusion rate of thiophene and *n*-heptane increase, resulting in an overall increase in thiophene and *n*-heptane molecules passing through the membrane. The partial flux of thiophene and *n*-heptane, as shown in Figure 5b, further confirms this speculation. (2) Increased temperature leads to PEG segment mobility, and the free volume of both membranes increases, further facilitating more thiophene and *n*-heptane to penetrate. The effect of temperature on the sulfur enrichment factor can be explained by solution and diffusion mechanisms. Permeation is controlled by the adsorption of thiophene at low temperatures. With increasing temperature, the adsorption of thiophene increases, thus enhancing the enrichment factor. When the temperature is above 75 °C, the permeation process is controlled by diffusion. Because the diffusion rate of *n*-heptane is higher than that of thiophene, the permeation ratio of thiophene to *n*-heptane decreases the enrichment factor.[37] To investigate the effect of temperature, the Arrhenius equation was used[38]

$$J_i = J_{0i} \exp\left(\frac{-E_p}{RT}\right) \quad (1)$$

where J_i (kg·m^{-2}·h^{-1}) is the fractional flux of thiophene and *n*-heptane, J_{0i} (kg·m^{-2}·h^{-1}) is the corresponding flux constant, E_p (kJ·mol^{-1}) is the activation energy of the pervaporation process, R is the molar gas constant (J·mol^{-1}·K^{-1}), and T (h)

https://dx.doi.org/10.1021/acsami.0c02513
ACS Appl. Mater. Interfaces 2020, 12, 20664–20671

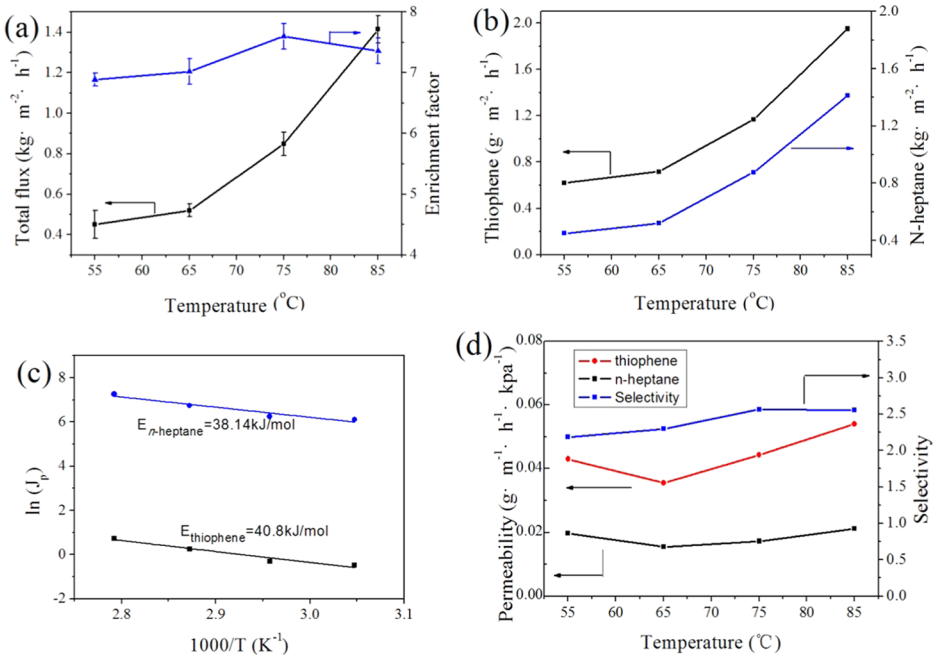

Figure 5. Effect of the operating temperature on the pervaporation performance of the PEG@ZIF-8/PVDF#6 membrane. Total flux and enrichment factor (a). Partial flux of thiophene and *n*-heptane (b). $\ln J - 10^3/T$ diagram (c). Permeability and selectivity with a normalized driving force (d).

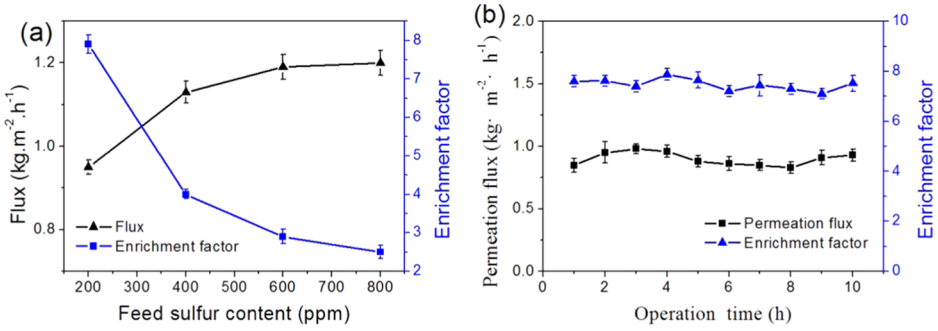

Figure 6. (a) Effect of the feed thiophene content on the performance of PEG@ZIF-8/PVDF#6 membrane. (b) Effect of operating time on the pervaporation performance of PEG@ZIF-8/PVDF#6 membrane.

is the reaction temperature. The natural logarithm of J has a linear relationship with the natural logarithm of T^{-1}. The values of J_{0i} and E_p for the thiophene/*n*-heptane mixture were obtained from the $\ln J - 10^3/T$ diagram shown in Figure 5c. Following this, we found that the E_p value of thiophene is generally higher than that of *n*-heptane, showing that thiophene permeation is more temperature-dependent. The normalized flux is usually expressed as the permeability (P_i), associated with the inherent properties of the membrane. This is measured by eq 2

$$P_i = l\frac{j_i}{P_{i0} - P_{il}} = l\frac{j_i}{\gamma_{i0}x_{i0}P_{i0}^{sat} - y_iP} \quad (2)$$

where x_{i0} and y_i are the mole fractions of component i in the feed liquid and permeate side, respectively, P_{i0}^{sat} is the feed saturated vapor pressure of component i, P is the total pressure in the system, and γ_{i0} is the activity coefficient on the feed concentration, found through reference literature or regression simulation (Aspen Plus 7.5).[39] The selectivity is defined as the ratio of the permeability of the two components as shown in eq 3. Selectivity is an inherent property of the membrane and effectively reflects the membrane performance.

The effect of temperature on the permeability and selectivity with a normalized driving

$$S = \frac{P_i}{P_j} = \frac{P_i/l}{P_j/l} \quad (3)$$

force is shown in Figure 5d. As feed temperature increases, the thiophene permeability decreases and *n*-heptane permeability increases, leading to the overall selectivity reduction with respect to temperature.

3.2.3. Effect of Feed Concentration. The influence of sulfur content on pervaporation performance was studied, and the result is shown in Figure 6a. The flux shows a relatively small change with increasing thiophene content, while the enrichment factor decreases. With an increase in feed thiophene content, the driving force increases owing to increasing thiophene activity and swelling of the composite membrane. However, this effect is minimal due to the strong association between the PEG and ZIF-8 layers. The adsorbed thiophene

https://dx.doi.org/10.1021/acsami.0c02513
ACS Appl. Mater. Interfaces 2020, 12, 20664−20671

achieves equilibrium, and no more preferential adsorption of thiophene occurs causing the enrichment factor to decrease.

3.2.4. Long-Term Operation Stability. It is common knowledge that the operation stability of membranes is an essential part of industrial application. To examine the stability of the prepared membrane, a long-time pervaporation desulfurization experiment of the PEG@ZIF-8/PVDF#6 membrane was performed, and the result is shown in Figure 6b. It can be seen that the total permeation flux and enrichment factor fluctuate within a narrow range, showing that the membrane performance is relatively stable. This result shows that the as-prepared desulfurization membrane has potential industrial application in the future.

3.2.5. Comparison of Desulfurization Performance. The comparison of the desulfurization of the as-prepared membrane in this study with recent studies[13,18,19,40−42] is shown in Figure 7. It can be seen that the enrichment factor of the membrane in this study is higher than that of other membranes reported previously, whereas the permeation flux of the membrane is lowest. This proves that the desulfurization of membrane can be enhanced by the introduction of the ZIF-8 layer, but the thicker ZIF-8 layers result in the decrease of permeation flux.

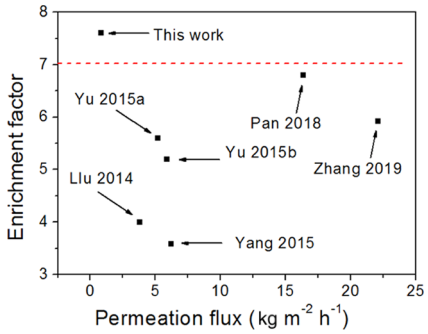

Figure 7. Comparison of various membranes from this and other studies.

4. CONCLUSIONS

The PEG@ZIF-8/PVDF nanocomposite membrane series were prepared via a layer-by-layer method. Characterization results indicated that the construction of PEG@ZIF-8/PVDF membranes could be adjusted by changing the number of growth cycles performed, and we used pervaporation experiment to evaluate the desulfurization properties of the composite membranes. The PEG@ZIF-8/PVDF#3 membrane has the highest permeation flux, reaching 3.08 kg·m^{-2}·h^{-1} at 85 °C. The dense ZIF-8 layer prevents the infiltration of the PEG solution and forms a uniform PEG separation layer, wherein both layers contribute to a higher sulfur enrichment factor with increasing growth cycles. The PEG@ZIF-8/PVDF#6 membrane has the highest sulfur enrichment factor, reaching 7.6 at 75 °C, which can be attributed to the unique membrane construction exerting a cooperative effect.

■ ASSOCIATED CONTENT

Supporting Information

The Supporting Information is available free of charge at https://pubs.acs.org/doi/10.1021/acsami.0c02513.

Schematic of the pervaporation apparatus; nitrogen sorption isotherms; pore size distribution; SEM image; TEM image; EDS mapping of ZIF-8/PVDF(#6) membrane surface and cross section; photos and micrographs of ZIF-8/PVDF#6 membrane after immersion into *n*-heptane/thiophene mixtures; schematic for ZIF-8 layers beneath PEG layer with increasing number of in situ growth cycles; and the surface and cross-sectional SEM of PEG@ZIF-8/PVDF membranes (PDF)

■ AUTHOR INFORMATION

Corresponding Authors

Xiaolong Han − *School of Chemical Engineering, Northwest University, Xi'an, Shaanxi 710069, China; Department of Chemistry, University of South Florida, Tampa, Florida 33620, United States; State Key Laboratory of Fine Chemicals, Dalian University of Technology, Dalian 116024, China*; Email: hanxl@nwu.edu.cn

Gaohong He − *State Key Laboratory of Fine Chemicals, Dalian University of Technology, Dalian 116024, China*; orcid.org/0000-0002-6674-8279; Email: hgaohong@dlut.edu.cn

Shengqian Ma − *Department of Chemistry, University of South Florida, Tampa, Florida 33620, United States*; orcid.org/0000-0002-1897-7069; Email: sqma@usf.edu

Authors

Hexiang Sun − *School of Chemical Engineering, Northwest University, Xi'an, Shaanxi 710069, China*

Zachary Magnuson − *Department of Chemistry, University of South Florida, Tampa, Florida 33620, United States*

Wenwen He − *Department of Chemistry, University of South Florida, Tampa, Florida 33620, United States*

Weijie Zhang − *Department of Chemistry, University of South Florida, Tampa, Florida 33620, United States*

Harsh Vardhan − *Department of Chemistry, University of South Florida, Tampa, Florida 33620, United States*; orcid.org/0000-0002-7131-7721

Complete contact information is available at: https://pubs.acs.org/10.1021/acsami.0c02513

Notes

The authors declare no competing financial interest.

■ ACKNOWLEDGMENTS

This work was supported by the State Key Laboratory of Fine Chemicals (KF1706), the Science and Technology Plan Projects of Shaanxi Province (2019GY-207), and the Postgraduate Independent Innovation Project of Northwest University (YZZ17135).

■ REFERENCES

(1) Rodenas, T.; Luz, I.; Prieto, G.; Seoane, B.; Miro, H.; Corma, A.; et al. Metal−Organic Framework Nanosheets in Polymer Composite Materials for Gas Separation. *Nat. Mater.* **2015**, *14*, 48−55.

(2) Hao, L.; Xiong, G.; Liu, L.; Long, H.; Jin, F.; Wang, X. Preparation of Highly Dispersed Desulfurization Catalysts and Their Catalytic Performance in Hydrodesulfurization of Dibenzothiophene. *Chin. J. Catal.* **2016**, *37*, 412−419.

(3) Soleimani, M.; Bassi, A.; Margaritis, A. Biodesulfurization of Refractory Organic Sulfur Compounds in Fossil Fuels. *Biotechnol. Adv.* **2007**, *25*, 570−596.

(4) Ma, X.; Velu, S.; Kim, J. H.; Song, C. Deep Desulfurization of Gasoline by Selective Adsorption over Solid Adsorbents and Impact of Analytical Methods on ppm-level Sulfur Quantification for Fuel Cell Applications. *Appl. Catal., B* **2005**, *56*, 137−147.
(5) Chica, A.; Corma, A.; Domine, M. E. Catalytic oxidative desulfurization (ODS) of diesel fuel on a continuous fixed-bed reactor. *J. Catal.* **2006**, *242*, 299−308.
(6) Yu, G.; Zhao, J.; Song, D.; Asumana, C.; Zhang, X.; Chen, X. Deep oxidative desulfurization of diesel fuels by acidic ionic liquids. *Ind. Eng. Chem. Res.* **2011**, *50*, 11690−11697.
(7) Zhang, Y.; Benes, N. E.; Lammertink, R. G. H. Performance study of pervaporation in a microfluidic system for the removal of acetone from water. *Chem. Eng. J.* **2016**, *284*, 1342−1347.
(8) Tsai, H. A.; Hsu, C. Y.; Huang, S. H.; Lee, K. R.; Hung, W. S.; et al. The preparation of polyelectrolyte/hydrolyzed polyacrylonitrile composite hollow fiber membrane for pervaporation. *J. Taiwan Inst. Chem. Eng.* **2018**, *91*, 623−633.
(9) Lin, L.; Kong, Y.; Wang, G.; Qu, H.; Yang, J.; Shi, D. Selection and crosslinking modification of membrane material for FCC gasoline desulfurization. *J. Membr. Sci.* **2006**, *285*, 144−151.
(10) Qi, R. B.; Wang, Y.; Chen, J.; Li, J. D.; Zhu, S. L. Removing thiophenes from n-octane using PDMS−AgY zeolite mixed matrix membranes. *J. Membr. Sci.* **2007**, *295*, 114−120.
(11) Li, B.; Dan, X.; Jiang, Z. Y.; Zhang, X.; Liu, W.; Xiao, D. Pervaporation performance of PDMS-Ni2+Y zeolite hybrid membranes in the desulfurization of gasoline. *J. Membr. Sci.* **2008**, *322*, 293−301.
(12) Wang, L.; Zhao, Z.; Li, J. D.; Chen, C. X. Synthesis and characterization of fluorinated polyimides for pervaporation of n-heptane/thiophene mixtures. *Eur. Polym. J.* **2006**, *42*, 1266−1272.
(13) Liu, K.; Fang, C. J.; Li, Z. Q.; Young, M. Separation of thiophene/n-heptane mixtures using PEBAX/PVDF-composited membranes via pervaporation. *J. Membr. Sci.* **2014**, *451*, 24−31.
(14) Yang, Z. J.; Zhang, W.; Li, J. D.; Chen, J. Polyphosphazene membrane for desulfurization: selecting poly[bis(trifluoroethoxy) phosphazene] for pervaporative removal of thiophene. *Sep. Purif. Technol.* **2012**, *93*, 15−24.
(15) Banerjee, R.; Phan, A.; Wang, B.; Knobler, C.; Furukawa, H.; O'Keeffe, M.; Yaghi, O. M. High-Throughput synthesis of zeolitic imidazolate frameworks and application to CO2 capture. *Science* **2008**, *319*, 939−943.
(16) Qasem, N. A. A.; Ben-Mansour, R.; Habib, M. A. An efficient CO2 adsorptive storage using MOF-5 and MOF-177. *Appl. Energy* **2018**, *210*, 317−326.
(17) Peng, Y. L.; Pham, T.; Li, P. L.; Wang, T.; Chen, Y.; Chen, K. J.; Forrest, K. A.; Space, B.; Cheng, P.; Zaworotko, M. J.; Zhang, Z. J. Robust ultramicroporous metal-organic frameworks with benchmark affinity for acetylene. *Angew. Chem., Int. Ed.* **2018**, *57*, 10971−10975.
(18) Yu, S.; Pan, F.; Yang, S.; Ding, H.; Jiang, Z.; Wang, B. Y.; et al. Enhanced pervaporation performance of MIL-101(Cr) filled polysiloxane hybrid membranes in desulfurization of model gasoline. *Chem. Eng. Sci.* **2015**, *135*, 479−488.
(19) Yu, S.; Jiang, Z. Y.; Ding, H.; Pan, F.; Wang, B. Y.; Yang, J.; Cao, X. Elevated pervaporation performance of polysiloxane membrane using channels and active sites of metal organic framework CuBTC. *J. Membr. Sci.* **2015**, *481*, 73−81.
(20) Guo, X.; Huang, H.; Ban, Y.; Yang, Q.; Xiao, Y.; Li, Y.; et al. Mixed matrix membranes incorporated with amine-functionalized titanium-based metal-organic framework for CO2/CH4 separation. *J. Membr. Sci.* **2015**, *478*, 130−139.
(21) Deng, Y.; Chen, J.; Chang, C.; Liao, K.; Tung, K.; Price, W. E.; et al. A drying-free, water-based process for fabricating mixed matrix membranes with outstanding pervaporation performance. *Angew. Chem., Int. Ed.* **2016**, *55*, 12793−12796.
(22) Han, X. L.; Hu, T. T.; Wang, Y.; Chen, H. Y.; Wang, Y. Q.; Yao, R. Q.; Ma, X.; Li, J. D.; Li, X. F. A water-based mixing process for fabricating ZIF-8/PEG mixed matrix membranes with efficient desulfurization performance. *Sep. Purif. Technol.* **2019**, *214*, 61−66.
(23) Wang, L. Y.; Fang, M. Q.; Liu, J.; He, J.; Li, J. D.; Lei, J. Layer-by-Layer fabrication of high-performance polyamide/ZIF-8 nanocomposite membrane for nanofiltration applications. *ACS Appl. Mater. Interfaces* **2015**, *7*, 24082−24093.
(24) Cravillon, J.; Münzer, S.; Lohmeier, S. J.; Feldhoff, A.; Huber, K.; Wiebcke, M. Rapid room-temperature synthesis and characterization of nanocrystals of a prototypical zeolitic imidazolate framework. *Chem. Mater.* **2009**, *21*, 1410−1412.
(25) Pokhrel, J.; Bhoria, N.; Anastasiou, S.; Tsoufis, T.; Gournis, D.; Romanos, G.; Karanikolos, G. N. CO2 adsorption behavior of amine-functionalized ZIF-8, graphene oxide, and ZIF-8/graphene oxide composites under dry and wet conditions. *Microporous Mesoporous Mater.* **2018**, *267*, 53−67.
(26) Jang, E.; Kim, E.; Kim, H.; Lee, T.; Yeom, H. J.; Kim, Y. W.; Choi, J. Formation of ZIF-8 membranes inside porous supports for improving both their H2/CO2, separation performance and thermal/mechanical stability. *J. Membr. Sci.* **2017**, *540*, 430−439.
(27) Bispo-Jr, A. G.; Oliveira, N. A.; Cardoso, C. X.; Lima, S. A. M.; Job, A. E.; Osorio-Roman, I. O.; Danna, C. S.; Pires, A. M. Red-light-emitting polymer composite based on PVDF membranes and Europium phosphor using Buriti Oil as plasticizer. *Mater. Chem. Phys.* **2018**, *217*, 160−167.
(28) Choi, M. H.; Yang, S. C. CoFe2O4 nanofiller effect on β-phase formation of PVDF matrix for polymer-based magnetoelectric composites. *Mater. Lett.* **2018**, *223*, 73−77.
(29) Liu, X. L.; Li, Y. S.; Ban, Y. J.; Peng, Y.; Jin, H.; Bux, H.; Xu, L. Y.; Caro, J.; Yang, W. S. Improvement of hydrothermal stability of zeolitic imidazolate frameworks. *Chem. Commun.* **2013**, *49*, 9140−9142.
(30) Gadipelli, S.; Travis, W.; Zhou, W.; Guo, Z. A thermally derived and optimized structure from ZIF-8 with giant enhancement in CO2 uptake. *Energy Environ. Sci.* **2014**, *7*, 2232−2238.
(31) Yang, Z. J.; Zhang, W.; Li, J. D.; Chen, J. Preparation and characterization of PEG/PVDF composite membranes and effects of solvents on its pervaporation performance in heptane desulfurization. *Desalin. Water Treat.* **2012**, *46*, 321−331.
(32) Yu, Z.; Bai, Y.; Zhang, S.; Liu, Y.; Zhang, N.; Wang, G. Metal-organic framework derived Co3ZnC/Co embedded in nitrogen doped CNT-grafted carbon polyhedra as high-performance electrocatalyst for water splitting. *ACS Appl. Mater. Interfaces* **2018**, *10*, 6245−6252.
(33) Nagaraju, D.; Bhagat, D. G.; Banerjee, R.; Kharul, U. K. In situ growth of metal-organic frameworks on a porous ultrafiltration membrane for gas separation. *J. Mater. Chem. A* **2013**, *1*, 8828−8835.
(34) Wei, W.; Xia, S.; Liu, G.; Dong, X.; Jin, W. Q.; Xu, N. Effects of polydimethylsiloxane (PDMS) molecular weight on performance of PDMS/ceramic composite membranes. *J. Membr. Sci.* **2011**, *375*, 334−344.
(35) Baheri, B.; Mohammadi, T. Sorption, diffusion and pervaporation study of thiophene/n-heptane mixture through self-support PU/PEG blend membrane. *Sep. Purif. Technol.* **2017**, *185*, 112−119.
(36) Mortaheb, H. R.; Ghaemmaghami, F.; Mokhtarani, B. A review on removal of sulfur components from gasoline by pervaporation. *Chem. Eng. Res. Des.* **2012**, *90*, 409−432.
(37) Hu, W.; Han, X.; Liu, L.; Zhang, X.; Xue, J.; Wang, B.; Zhang, P.; Cao, X. Z. PEG/PVDF membranes for separating organosulphur compounds from n-heptane: Effect of PEG molecular weight. *Can. J. Chem. Eng.* **2017**, *95*, 364−371.
(38) Chaudhari, S.; Kwon, Y. S.; Moon, M. J.; Shon, M. Y.; Park, Y. I.; Song, H. R.; et al. Water-selective membrane from crosslinking of poly(vinyl alcohol) with aartaric acid and its pervaporation separation characteristics for a water/acetic acid mixture. *Bull. Korean Chem. Soc.* **2015**, *36*, 2534−2541.
(39) Guo, B.; Bai, J.; Li, Y.; Xia, S.; Ma, P. Isobaric vapor−liquid equilibrium for four binary systems of 3-methylthiophene. *Fluid Phase Equilib.* **2012**, *320*, 26−31.
(40) Yang, D.; Yang, S.; Jiang, Z. Y.; Yu, S. N.; Zhang, J. L.; Pan, F. S.; Cao, X. Z.; Wang, B. Y.; Yang, J. Polydimethylsiloxane−graphene

https://dx.doi.org/10.1021/acsami.0c02513
ACS Appl. Mater. Interfaces 2020, 12, 20664−20671

nanosheets hybrid membranes with enhanced pervaporative desulfurization performance. *J. Membr. Sci.* **2015**, *487*, 152−161.
(41) Pan, F. S.; Wang, M. D.; Ding, H.; Song, Y. M.; Li, W. D.; Wu, H.; Jiang, Z. Y.; Wang, B. Y.; Cao, X. Z. Embedding Ag+@COFs within Pebax membrane to confer mass transport channels and facilitated transport sites for elevated desulfurization performance. *J. Membr. Sci.* **2018**, *552*, 1−12.
(42) Zhang, Y.; Jiang, Z. Y.; Song, J.; Pan, F. S.; Zhang, P.; Cao, X. Z.; et al. Elevated pervaporative desulfurization performance of Pebax-Ag+@MOFs hybrid membranes by integrating multiple transport mechanisms. *Ind. Eng. Chem. Res.* **2019**, *58*, 16911−16921.

https://dx.doi.org/10.1021/acsami.0c02513
ACS Appl. Mater. Interfaces 2020, 12, 20664−20671